Journal of Sound and Vibration (1999) **221**(4), 545–565
Article No. jsvi.1998.2045, available online at http://www.idealibrary.com on IDEAL

CONTROLLING THE ATTITUDE MANEUVERS OF FLEXIBLE SPACECRAFT BY USING TIME-OPTIMAL/FUEL-EFFICIENT SHAPED INPUTS

S. PARMAN and H. KOGUCHI
Department of Mechanical Engineering, Nagaoka University of Technology, Japan

(*Received* 8 *April* 1998, *and in final form* 8 *October* 1998)

A three-dimensional rest-to-rest attitude maneuver of flexible spacecraft equipped with on–off reaction jets is studied. Equations of motion of the spacecraft are developed by using Lagrangian formulation. The finite element method is used to discretize elastic deformations of a particular model of satellite with flexible solar panels by modelling the panels as flat plate structures in bending. Under unshaped inputs, the maneuvers induce an undesirable motion of the satellite as well as vibration of the solar panels. Time-optimal and fuel-efficient input shapers are then applied to reduce the residual oscillation of its motion at several natural frequencies in order to get an expected pointing precision of the satellite. Once the shaped inputs are given to the satellite, the performance improves significantly. Results indicate that, the fuel-efficient shaped inputs give smaller maximum deflections of flexible members compared with the time-optimal ones.

1. INTRODUCTION

A spacecraft designed to have a certain orientation relative to the earth, for example, needs a reorientation of its attitude after reaching a geostationary orbit or frequent attitude corrections during its operation. Attitude maneuver of rigid spacecraft can be done without a lot of vibration problems after reaching its desired attitude. For a flexible spacecraft maneuvering the attitude without regard to system flexibility or without controls on the flexible members, large amplitude transient and steady-state oscillations may occur, especially when the system is equipped with on–off jets. Such a system often needs an attitude maneuver with limited vibration both during and after the maneuver. For example, it may be necessary to generate a torque profile such that the flexible spacecraft is rotated through a desired attitude angle with its residual oscillation in a permissible value, while the deflections of flexible members remain small throughout the maneuver and go to zero at the end of the maneuver.

The technique of input shaping to minimize modal vibration in slew maneuvers of a flexible spacecraft system has received much attention in the recent few years. Input shaping is implemented by convolving a sequence of

0022–460X/99/040545 + 21 $30.00/0

impulses, an input shaper, with a desired system command to produce a shaped input that is then used to drive the system [1]. The amplitudes and time locations of the impulses are determined by solving a set of constraint equations formulated to control the dynamic performance of the system.

Flexible spacecraft equipped with on–off reaction jets cannot produce the variable-ampliftude actuation force that is usually required with input shaping. The spacecraft is controlled with constant-amplitude force pulses. Rogers and Seering [2] developed the method for extending input shaping to the case of on–off actuators. Constraints on the impulse amplitudes have been used to generate time-optimal command profiles for on–off reaction jets. A lot of studies [3–5] have demonstrated on–off input shaping with mass, spring, and damper simulations. These studies have concentrated on eliminating residual vibration. No constraints were placed on the amplitude of deflection during the slew. Pao and Singhose [6] have shown that input shaping is very successful in eliminating residual vibration and has the benefit of decreasing transient deflection when compared to bang-bang control. However, the amplitude of the transient deflection is not limited and can still be very large. Singhose *et al*. [7] studied input shaping to observe slew maneuvers of flexible spacecraft with the limitation on member deflection. They modelled the spacecraft as a spring–mass system, both for rotary and linear systems. For such simple models with one flexible mode and a rigid-body mode, expressions for the deflection of the systems can be derived easily. But for systems with a lot of flexible modes, the derivation of their expressions becomes very troublesome.

A spacecraft or a satellite in operation needs certain accuracies in its attitude. The KOREASAT requires a satellite with an antenna beam pointing error not greater than 0·07° in roll and pitch, and not more than 0·2° in yaw [8]. Owing to such criteria, the flexible satellite maneuvered by shaped inputs must have residual attitude oscillation that does not surpass the permissible maximum error. However, for a system having a lot of flexible modes, such as the finite element model of a satellite with flexible solar panels studied by Koguchi and Parman [9–11], when the satellite is subjected to a shaped input suppressing residual vibration at the frequency with the highest vibration amplitude, other frequencies can amplify the resulting residual vibration so that the satellite attitude oscillation after maneuver is still greater than the permissible attitude error. In this case, shaped inputs suppressing residual vibration at several frequencies are needed.

This paper presents computer simulations of rest-to-rest attitude maneuvers of a satellite with flexible solar panels under shaped inputs. The equation of motion is derived by using a hybrid system of co-ordinates and a Lagrange's formulation, and the finite element method is used to discretize elastic deformations of solar panels by modelling them as flat plate structures in bending, such as the model proposed by Koguchi and Parman [9–11]. The time-optimal and fuel-efficient shaped inputs are selected to make zero vibration at the frequency with the greatest amplitude of residual attitude oscillation and small vibration at several other frequencies in order to control the attitude maneuvers of the satellite. This is so that its residual attitude oscillation is a

permissible value at the end of maneuvers, while the deflections of solar panels during the maneuvers are still small.

2. MATHEMATICAL FORMULATION OF FLEXIBLE SPACECRAFT DYNAMICS

The particular spacecraft being studied in this paper is a satellite containing a rigid main body and two symmetrical flexible solar panels, as shown in Figure 1. To identify the satellite attitude relative to an inertial frame $F_i(O_iX_iY_iZ_i)$, a main body fixed frame $F_b(O_bX_bY_bZ_b)$ is defined. To discretize elastic deformations of the panels, the finite element method (FEM) is used. For this application, each solar panel is divided into 16 rectangular bending plate elements. The elements on the right side are numbered from 1 to 16 and on the left side from 17 to 32, while their nodal points are numbered from 1 to 27 and from 28 to 54. Displacements of their nodes are measured in substructure reference frames $F_j(O_jX_jY_jZ_j)$ ($j = 1, 2, \ldots, 32$). The Y_j-axes ($j = 1, 2, \ldots, 16$) of the right side panel are parallel to the Y_b-axis, while the Y_j-axes ($j = 17, 18, \ldots, 32$) of the left side are anti-parallel. All Z_j-axes are normal to their panels. The origin of the main body fixed frame O_b is placed on the mid-point of the longitudinal axis of the solar panels. The solar panels are oriented towards the sun, and the declination with respect to the X_b-axis is identified by the offset angle δ.

2.1. GENERAL EQUATIONS OF MOTION OF FLEXIBLE SPACECRAFT

In this section, the mathematical model of general gravity oriented and non-spinning flexible spacecraft dynamics will be derived by using a Lagrangian formulation, so that the expressions of kinetic energy and potential energy for the whole spacecraft need to be determined first. Since the spacecraft considered consists of the rigid main body and several flexible substructures, the kinetic energy and potential energy of the spacecraft can be determined by observing the rigid body and flexible structural subsystems separately, and then summing their resulted kinetic and potential energies.

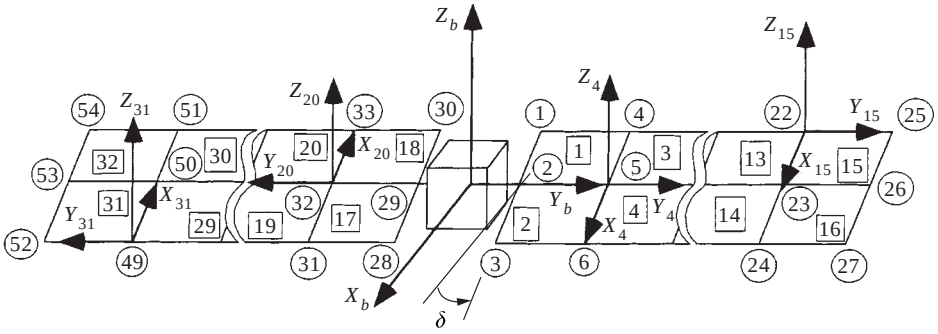

Figure 1. The model of the satellite being investigated; element numbering, nodal point numbering, rigid main body fixed reference frame, and local reference frames.

2.1.1. *Kinetic energy*

The kinetic energy of the rigid main body of the spacecraft can be written in the following form:

$$E_{k_b} = \tfrac{1}{2}\dot{\mathbf{r}}_{i,b}^T\dot{\mathbf{r}}_{i,b}m_b + \tfrac{1}{2}\boldsymbol{\omega}_{b,i}^T\mathbf{I}_b\boldsymbol{\omega}_{b,i} + \dot{\mathbf{r}}_{i,b}^T\mathbf{Q}_b\boldsymbol{\omega}_{b,i}, \tag{1}$$

where $\mathbf{r}_{i,b}$ is a vector from O_i to O_b with the overdot indicating its differentiation with respect to time relative to F_i, $\boldsymbol{\omega}_{b,i}$ is the angular velocity vector of F_b relative to F_i, m_b is the total mass of the main body, $\mathbf{I}_b$ is the inertia matrix of the body relative to O_b, and $\mathbf{Q}_b$ is the coupling matrix between translational and rotational displacements of the main body. If O_b coincides with the centre of mass of the main body, the value of $\mathbf{Q}_b$ equals zero.

The kinetic energy of flexible substructures, by following the finite element method [12], can be written in the following form:

$$E_{ka} = \tfrac{1}{2}\dot{\mathbf{r}}_{i,b}^T\dot{\mathbf{r}}_{i,b}m_a + \tfrac{1}{2}\dot{\mathbf{d}}^T\mathbf{M}\dot{\mathbf{d}} + \tfrac{1}{2}\boldsymbol{\omega}_{b,i}^T\mathbf{I}_a\boldsymbol{\omega}_{b,i} + \boldsymbol{\omega}_{b,i}^T\mathbf{A}\dot{\mathbf{d}} + \dot{\mathbf{r}}_{i,b}^T\mathbf{W}\dot{\mathbf{d}} + \dot{\mathbf{r}}_{i,b}^T\mathbf{Q}_a\boldsymbol{\omega}_{b,i}, \tag{2}$$

where $\mathbf{d}$ is the displacement vector of flexible substructures, m_a is the mass of substructures, $\mathbf{M} = \sum_{j=1}^{N}\mathbf{P}_j^T\mathbf{M}_j\mathbf{P}_j$ is its mass matrix, and $\mathbf{I}_a = \sum_{j=1}^{N}\mathbf{T}_j^T\mathbf{I}_j\mathbf{T}_j$ is its inertia matrix with respect to O_b. The coupling matrices $\mathbf{A} = \sum_{j=1}^{N}\mathbf{T}_j^T\mathbf{A}_j\mathbf{P}_j$ and $\mathbf{W} = \sum_{j=1}^{N}\mathbf{T}_j^T\mathbf{W}_j\mathbf{P}_j$ relate the main body rotational and translational displacements respectively to the substructure displacements, while $\mathbf{Q}_a = \sum_{j=1}^{N}\mathbf{T}_j^T\mathbf{Q}_j\mathbf{T}_j$ is the coupling matrix between the translational and rotational displacements of the main body contributed by the undeformed-state substructures. In these matrices, N is the number of elements of flexible substructures. For the jth element, $\mathbf{T}_j$ is the transformation matrix from F_b to F_j, $\mathbf{P}_j$ is the assembling matrix relating the element displacement vector $\mathbf{d}_j$ and the displacement vector of flexible substructures $\mathbf{d}$ in the form of $\mathbf{d}_j = \mathbf{P}_j\mathbf{d}$, $\mathbf{M}_j = \int_{m_j}\mathbf{C}_j^T\mathbf{C}_j\,\mathrm{d}m$ is the mass matrix, $\mathbf{A}_j = {}^j\tilde{\mathbf{r}}_{b,o}\mathbf{W}_j + \int_{m_j}{}^j\tilde{\mathbf{r}}_{o,p_0}\mathbf{C}_j\,\mathrm{d}m$ and $\mathbf{W}_j = \int_{m_j}\mathbf{C}_j\,\mathrm{d}m$ are the coupling matrices between rotational and translational displacements of the main body respectively and the element displacements, $\mathbf{Q}_j = \int_{m_j}({}^j\tilde{\mathbf{r}}_{b,o} + {}^j\tilde{\mathbf{r}}_{o,p_0})^T\,\mathrm{d}m$ is the coupling matrix for the translational and rotational displacements of the main body contributed by the undeformed-state element, and $\mathbf{I}_j = \int_{m_j}({}^j\tilde{\mathbf{r}}_{b,o} + {}^j\tilde{\mathbf{r}}_{o,p_0})^T({}^j\tilde{\mathbf{r}}_{b,o} + {}^j\tilde{\mathbf{r}}_{o,p_0})\,\mathrm{d}m$ is the element inertia matrix with respect to O_b. $\mathbf{C}_j$ is the element shape function matrix, ${}^j\mathbf{r}_{b,\,o}$ and ${}^j\mathbf{r}_{o,p_0}$ are vectors from O_b to O_j and from O_j to a particle p with mass $\mathrm{d}m$ of the element in the undeformed state respectively expressed in F_j, while a general notation of $\tilde{\mathbf{r}}$ means the skew symmetric matrix of a vector $\mathbf{r}$.

2.1.2. *Potential energy*

The potential energy of the satellite consists of the potential energy of its undeformed state and the potential energy due to elastic deformations of flexible substructures. The potential energy of the undeformed state, in this research, is measured relative to the earth. When the satellite orbit is circular, it can be expressed as

$$E_{pr} = E_{pr}(\mathbf{r}_{i,b}). \tag{3}$$

The potential energy due to elastic deformations is the sum of the strain energy of flexible substructures and the potential energy due to external forces acting on the substructures with a minus sign. By following the general finite element method procedures, the potential energy due to the elastic deformations of flexible substructures can be written in the following form:

$$E_{pa} = \tfrac{1}{2}\mathbf{d}^T\mathbf{K}\mathbf{d} - \mathbf{d}^T\mathbf{F}_a, \tag{4}$$

where $\mathbf{K} = \sum_{j=1}^{N} \mathbf{P}_j^T\mathbf{K}_j\mathbf{P}_j$ is the stiffness matrix of the substructures and $\mathbf{F}_a = \sum_{j=1}^{N} \mathbf{P}_j^T\mathbf{f}_j$ is the discrete external forces vector acting on the substructures. For the jth element, $\mathbf{f}_j = \int_{V_j} \mathbf{C}_j^T\mathbf{F}_f \, \mathrm{d}V$ is the discrete external forces vector acting on the nodes and $\mathbf{K}_j = \int_{V_j} \mathbf{C}_j^T\mathbf{B}_j^T\mathbf{R}_j\mathbf{B}_j\mathbf{C}_j \, \mathrm{d}V$ is the stiffness matrix. $\mathbf{F}_f$ is a distributed external forces vector working on the element, $\mathbf{B}_j$ is an operator matrix containing first or second order derivative operators, and $\mathbf{R}_j$ is an elasticity matrix of element j.

2.1.3. *Equations of motion*

To derive the general equations of motion of flexible spacecraft by using the Lagrangian procedure, the Lagrangian operator and Lagrange's equation of motion are used. Then, it is assumed that control (external) forces acting on the rigid main body of the spacecraft are much larger than the forces resulting from the potential energy of the undeformed state. By using equations (1)–(4), the equations of motion of the spacecraft can then be written in the linearized form as follows:

$$\begin{bmatrix} m\mathbf{U}_3 & \mathbf{Q} & \mathbf{W} \\ \mathbf{Q}^T & \mathbf{I} & \mathbf{A} \\ \mathbf{W}^T & \mathbf{A}^T & \mathbf{M} \end{bmatrix} \begin{Bmatrix} \ddot{\mathbf{r}} \\ \ddot{\boldsymbol{\Theta}} \\ \ddot{\mathbf{d}} \end{Bmatrix} + \begin{bmatrix} \mathbf{0} & \mathbf{Q}\tilde{\boldsymbol{\omega}}_0 & \mathbf{0} \\ \mathbf{0} & \mathbf{I}\tilde{\boldsymbol{\omega}}_0 & \mathbf{0} \\ \mathbf{0} & \mathbf{A}^T\tilde{\boldsymbol{\omega}}_0 & \mathbf{D} \end{bmatrix} \begin{Bmatrix} \dot{\mathbf{r}} \\ \dot{\boldsymbol{\Theta}} \\ \dot{\mathbf{d}} \end{Bmatrix}$$

$$+ \begin{bmatrix} \mathbf{0} & \mathbf{0} & \mathbf{0} \\ \mathbf{0} & \mathbf{0} & \mathbf{0} \\ \mathbf{0} & \mathbf{0} & \mathbf{K} \end{bmatrix} \begin{Bmatrix} \mathbf{r} \\ \boldsymbol{\Theta} \\ \mathbf{d} \end{Bmatrix} = \begin{Bmatrix} \mathbf{F}_b \\ \mathbf{T}_b \\ \mathbf{F}_a \end{Bmatrix}, \tag{5}$$

where $\mathbf{F}_b$ and $\mathbf{T}_b$ are external forces and torques vectors acting on the main body, $\mathbf{D}$ is the damping matrix of the substructures, $\boldsymbol{\omega}_0$ and $\boldsymbol{\Theta}$ are orbital velocity and attitude angles vector of the satellite, respectively. In this paper, the attitude angles are expressed in Bryant angles (roll ϕ, pitch θ, and yaw ψ). Also, the flexible structural subsystems are assumed to have no dissipation properties, or $\mathbf{D} = \mathbf{0}$.

2.2. PARTICULAR DYNAMICAL MODEL OF THE SATELLITE WITH SOLAR PANELS BEING MODELLED AS RECTANGULAR PLATE ELEMENTS.

The mathematical expression of general spacecraft dynamics has been formed in equation (5). In this section, a particular model of flexible spacecraft—a satellite consisting of a rigid main body carrying two symmetrical flexible solar panels—will be developed. However, equation (5) needs to be evaluated for a certain type of flexible substructures. In this study, the attitude of the

hypothetical satellite being chosen is as follows: the Z_b-axis of the rigid main body reference frame should point to the centre of the earth, the Y_b-axis is normal to the orbital plane, and the X_b-axis should point to the velocity when there are no attitude errors.

For the application of the finite element method to discretize elastic deformations of solar panels, the following idealizations are used: (1) the solar panels are divided into rectangular flat plate bending elements, (2) each element has a uniform mass density, (3) only out-of-plane deformations of solar panels are considered, (4) external loads (both forces and torques) on the solar panels are assumed to work on the nodal points of the elements, and (5) the Y_j-axes of elements and the Y_b-axis of the main body frame are parallel or antiparallel. The X_j-axes and Y_j-axes of elements are in the panel plane, and their Z_j-axes are normal to the plane. By using the above idealizations, each element of the solar panel has 12 degrees of freedom in total, as shown in Figure 2.

In this research, the material of the solar panels is assumed to be isotropic material. For an isotropic plate, $\mathbf{R}_j$ can be written as

$$\mathbf{R}_j = \frac{Et^3}{12(1-\nu^2)} \begin{bmatrix} 1 & \nu & 0 \\ \nu & 1 & 0 \\ 0 & 0 & \dfrac{1-\nu}{2} \end{bmatrix}, \tag{6}$$

where E, t, and ν are the element Young's modulus, thickness, and Poisson's ratio, respectively. The shape function matrix introduced by Bogner *et al.* [13] is selected. This shape function matrix can guarantee that deflections and slopes are continuous at all edges of the element. Its expression for the jth element is as follows:

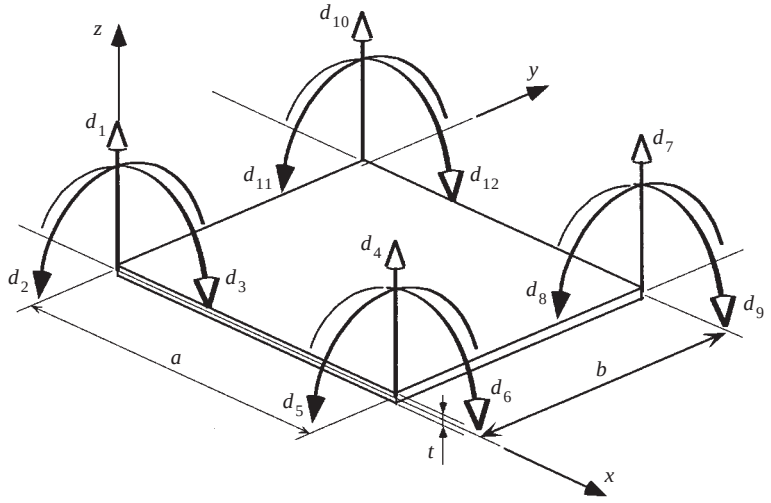

Figure 2. A rectangular plate bending element model of the solar panel.

$$\mathbf{C}_j^T = \begin{bmatrix} (1+2\xi)(1-\xi)^2(1+2\eta)(1-\eta)^2 \\ (1+2\xi)(1-\xi)^2\eta(1-\eta)^2 b \\ -\xi(1-\xi)^2(1+2\eta)(1-\eta)^2 a \\ (1+2\xi)(1-\xi)^2(3-2\eta)\eta^2 \\ -(1+2\xi)(1-\xi)^2(1-\eta)\eta^2 b \\ -\xi(1-\xi)^2(3-2\eta)\eta^2 a \\ (3-2\xi)\xi^2(3-2\eta)\eta^2 \\ -(3-2\xi)\xi^2(1-\eta)\eta^2 b \\ (1-\xi)\xi^2(3-2\eta)\eta^2 a \\ (3-2\xi)\xi^2(1+2\eta)(1-\eta)^2 \\ (3-2\xi)\xi^2\eta(1-\eta)^2 b \\ (1-\xi)\xi^2(1+2\eta)(1-\eta)^2 a \end{bmatrix}, \tag{7}$$

where a and b are the element length and width, respectively, $\xi = x/a$, and $\eta = y/b$. For this shape function matrix, the coupling matrix $\mathbf{A}_j$ can be obtained as follows:

$$\mathbf{A}_j^T = \frac{\rho tab}{24} \begin{bmatrix} 6y_{0j} + \frac{9}{5}b & -6x_{0j} - \frac{9}{5}a & 0 \\ by_{0j} + \frac{2}{5}b^2 & -bx_{0j} - \frac{3}{10}ab & 0 \\ -ay_{0j} - \frac{3}{10}ab & ax_{0j} + \frac{2}{5}a^2 & 0 \\ 6y_{0j} + \frac{21}{5}b & -6x_{0j} - \frac{9}{5}a & 0 \\ -by_{0j} - \frac{3}{5}b^2 & bx_{0j} + \frac{3}{10}ab & 0 \\ -ay_{0j} - \frac{7}{10}ab & ax_{0j} + \frac{2}{5}a^2 & 0 \\ 6y_{0j} + \frac{21}{5}b & -6x_{0j} - \frac{21}{5}a & 0 \\ -by_{0j} - \frac{3}{5}b^2 & bx_{0j} + \frac{7}{10}ab & 0 \\ ay_{0j} + \frac{7}{10}ab & -ax_{0j} - \frac{3}{5}a^2 & 0 \\ 6y_{0j} + \frac{9}{5}b & -6x_{0j} - \frac{21}{5}a & 0 \\ by_{0j} + \frac{2}{5}b^2 & -bx_{0j} - \frac{7}{10}ab & 0 \\ ay_{0j} + \frac{3}{10}ab & -ax_{0j} - \frac{3}{5}a^2 & 0 \end{bmatrix}, \tag{8}$$

where x_{0j} and y_{0j} are components of the vector from O_b to O_j in the X_j-axis and Y_j-axis directions respectively. The inertia matrix $\mathbf{I}_j$ can be written as follows:

$$\mathbf{I}_j = \rho abt \begin{bmatrix} I_{j,11} & I_{j,21} & I_{j,31} \\ I_{j,21} & I_{j,22} & I_{j,32} \\ I_{j,31} & I_{j,32} & I_{j,33} \end{bmatrix}, \tag{9}$$

where

$$I_{j,11} = y_{0j}^2 + \tfrac{1}{12}t^2 + \tfrac{1}{3}b^2 + y_{0j}b, \tag{10a}$$

$$I_{j,21} = -\tfrac{1}{2}(\tfrac{1}{2}ab + y_{0j}a + x_{0j}b) - x_{0j}y_{0j}, \tag{10b}$$

$$I_{j,31} = I_{j,32} = 0, \tag{10c}$$

$$I_{j,22} = x_{0j}^2 + \tfrac{1}{12}t^2 + \tfrac{1}{3}a^2 + x_{0j}a, \tag{10d}$$

$$I_{j,33} = x_{0j}^2 + y_{0j}^2 + \tfrac{1}{3}(a^2 + b^2) + x_{0j}a + y_{0j}b, \tag{10e}$$

and the coupling matrix for rotational displacements of the main body and the displacements of element j can be written as follows:

$$\mathbf{W}_j = \frac{\rho tab}{24} = \begin{bmatrix} 0 & 0 & 0 & 0 & 0 & 0 & 0 & 0 & 0 & 0 & 0 & 0 \\ 0 & 0 & 0 & 0 & 0 & 0 & 0 & 0 & 0 & 0 & 0 & 0 \\ 6 & b & -a & 6 & -b & -a & 6 & -b & a & 6 & b & a \end{bmatrix}. \tag{11}$$

3. REST-TO-REST THREE-DIMENSIONAL ATTITUDE MANEUVER OF FLEXIBLE SATELLITE UNDER BANG-BANG TORQUE INPUTS

In this study, the observed satellite is supposed to have no control and no damping properties on the flexible solar panels. The control inputs are only applied to the rigid main body, at the center of the mass of the satellite, as on–off reaction jets with constant amplitude force or torque pulses. For such a system, under control or external torques only, considering equation (5), the resulted attitude angle acceleration of the satellite as a rigid body motion can be written as

$$\begin{Bmatrix} \ddot{\phi} \\ \ddot{\theta} \\ \ddot{\psi} \end{Bmatrix} = \begin{bmatrix} I_x & I_{xy} & I_{xz} \\ I_{xy} & I_y & I_{yz} \\ I_{xz} & I_{yz} & I_z \end{bmatrix}^{-1} \begin{Bmatrix} T_{b_x} \\ T_{b_y} \\ T_{b_z} \end{Bmatrix}, \tag{12}$$

where I_x, I_y, I_z, I_{xy}, I_{xz}, and I_{yz} are components of the inertia matrix $\mathbf{I}$ of the whole satellite, and T_{b_x}, T_y, and T_{b_z} are components of the torque input vector $\mathbf{T}_b$ on the rigid main body. By integrating equation (12) with respect to time one gets an expression of desired attitude angle velocity:

$$\begin{Bmatrix} \dot{\phi}_d \\ \dot{\theta}_d \\ \dot{\psi}_d \end{Bmatrix} = \int \begin{bmatrix} I_x & I_{xy} & I_{xz} \\ I_{xy} & I_y & I_{yz} \\ I_{xz} & I_{yz} & I_z \end{bmatrix}^{-1} \begin{Bmatrix} T_{b_x} \\ T_{b_y} \\ T_{b_z} \end{Bmatrix} \mathrm{d}t, \tag{13}$$

and integrating once more gives a desired roll angle displacement:

$$\begin{Bmatrix} \phi_d \\ \theta_d \\ \psi_d \end{Bmatrix} = \iint \begin{bmatrix} I_x & I_{xy} & I_{xz} \\ I_{xy} & I_y & I_{yz} \\ I_{xz} & I_{yz} & I_z \end{bmatrix}^{-1} \begin{Bmatrix} T_{b_x} \\ T_{b_y} \\ T_{b_z} \end{Bmatrix} \mathrm{d}t\, \mathrm{d}t. \tag{14}$$

TABLE 1
Lumped masses consisting of the rigid main body

Mass (kg)	Position (X_b, y_b, z_b) (m)
400	(0·40, 0·00, 0·00)
400	(−0·40, 0·00, 0·00)
500	(0·00, 0·50, 0·00)
500	(0·00, −0·50, 0·00)
550	(0·00, 0·00, 1·40)
550	(0·00, 0·00, −1·40)

The main body of the satellite is modelled as six lumped masses at certain positions, shown in Table 1, the parameters of the flexible solar panels being used can be seen in Table 2. The offset angle of solar panels δ is taken to be 30°. For this configuration, O_b coincides with the centre of the mass of the whole satellite in the undeformed state, $I_x = 17\,535$ kg-m^2, $I_y = 2384$ kg-m^2, $I_z = 15\,557$ kg-m^2, $I_{xy} = I_{yz} = 0$, and $I_{xz} = 43$ kg-m^2. The initial condition of the observed satellite is an undeformed state and F_b coincides with F_i. The satellite is orbiting the earth in a constant angular velocity

$$\boldsymbol{\omega}_0 = -7{\cdot}29\ 10^{-5}\,\mathbf{j}_i \text{ rad/s}, \tag{15}$$

where $\mathbf{j}_i$ is the unit vector in the Y_i-axis direction. This means that F_b performs in F_i one rotation per sidereal day (24 h of sidereal time or 23 h 56 min 4·09054 s of mean solar time).

The roll angle of the satellite will be changed to the desired angle 5°, or about 0·0873 rad, while the pitch and yaw angles are still 0°. The constant-amplitude command for rest-to-rest slew maneuver in the shortest duration time is a bang-bang input. Constraint equations that must be satisfied for this rest-to-rest slew maneuver are $\{\dot{\phi}_d, \dot{\theta}_d, \dot{\psi}_d\}^T = \mathbf{0}$ and $\{\phi_d, \theta_d, \psi_d\}^T = \{0{\cdot}0873, 0, 0\}^T$. If the amplitude of command, either T_{b_x}, T_{b_y}, or T_{b_z}, applied on the satellite is 20 N-m,

TABLE 2
Parameters of the solar panels of the satellite

Description	Values
Number of solar panels	2
Dimension of each solar panel (m)	$12 \times 2{\cdot}4 \times 0{\cdot}03$
Young's modulus, E (N/m^2)	$0{\cdot}6 \times 10^8$
Poisson ratio ν	0·3
Mass density, ρ(kg/m^3)	120
Number of elements in each solar panel	16
Dimension of each element, $b \times a \times t$ (m)	$1{\cdot}5 \times 1{\cdot}2 \times 0{\cdot}03$
Offset angle, δ (degrees)	30
Distance between panel's root and O_b (m)	1·80

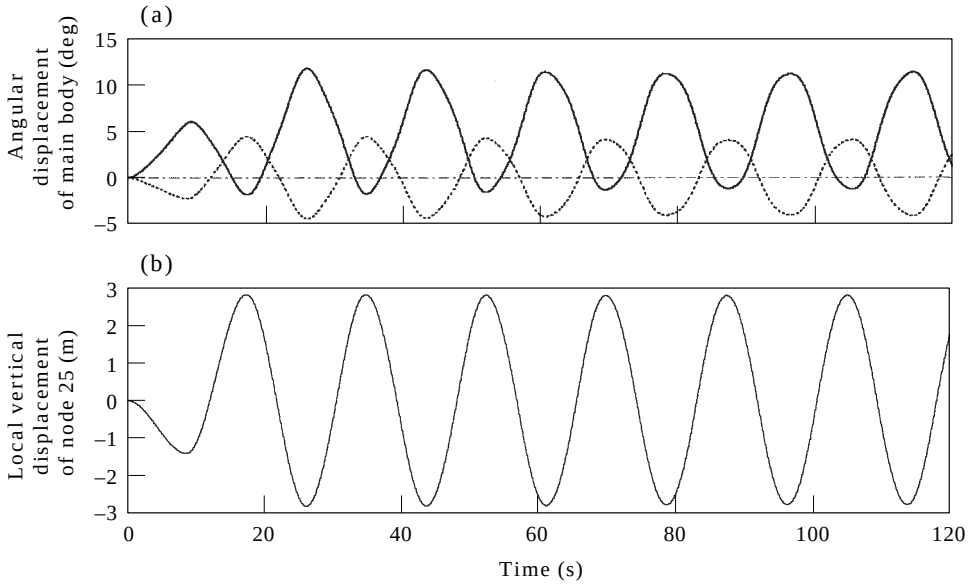

Figure 3. Time responses under the bang-bang roll and yaw torque inputs: (a) attitude angle displacement of the main body; (b) vertical displacement measured in the local reference frame of node 25 of the solar panel. —, Roll; - · - ·, pitch, - - - - -, yaw.

the profile of bang-bang torques needed consists of 17·494 s of T_{b_x} and 0·868 s of T_{b_z} bang-bangs. The satellite is subjected firstly to the roll torque input only, and after that, the yaw input is applied. Under these inputs, the roll angle changes to the desired displacement, the yaw angle is disturbed, while the pitch angle is not excited. After the inputs are stopped, the roll and yaw angles still oscilate in very large amplitudes dominantly at the period of 17·49 s (i.e., at the natural frequency of 0·3593 rad/s). The resultant amplitude of residual roll angle oscillation is 6·76°, while the resultant amplitude of residual yaw angle oscililation is 4·47° as shown in Figure 3(a). This means that the residual roll angle oscillation is about 135% of the desired roll displacement. Of course such residual oscillation is unfavorable and may disturb the satellite mission. The solar panels vibrate in very large amplitudes. The largest residual vibrations occur at their tips. Node 25 experiences an unlikely local vertical vibration, where the large amplitude of 2·847 m occurs, as shown in Figure 3(b). Compared with the solar panel's length of 12 m, this amplitude of vibration is about 24%. For such conditions the use of the local reference frame fixed at the undeformed-state element in the finite element method is no longer true.

The influence of the bang-bang yaw command applied to residual attitude angle oscillations of the satellite, in this case, is very small. If the satellite is subjected to this yaw command only, the total amplitudes of residual roll and yaw angle oscillations are less then 0·04° and 0·03°, respectively as shown in Figure 4, while the pitch angle is undisturbed. The pitch angle is still zero.

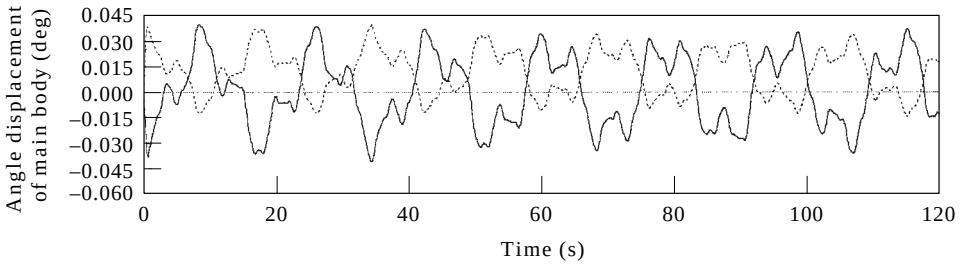

Figure 4. Time responses of the rigid main body under the bang-bang yaw torque input only. Key as for Figure 3.

4. INPUT SHAPERS TO REDUCE RESIDUAL VIBRATION IN REST-TO-REST ATTITUDE MANEUVERS

The flexible satellite studied here is equipped with on–off reaction jets, and so cannot produce a variable-amplitude actuation force. The satellite must be moved with constant-amplitude force pulses. For this kind of satellite, when the bang-bang input is used for rest-to-rest slew maneuvers, the resulting residual vibration of flexible members and attitude oscillation of the rigid main body can be relatively large compared with the desired new attitude. By shaping the input, the residual vibration can be reduced.

The command inputs applied to the observed satellite consist of positive or negative constant-amplitude force pulses. For rest-to-rest maneuvers, the commands must contain both positive and negative pulses so that the satellite can be accelerated and then decelerated back to zero velocity. Two kinds of profiles can be generated by these inputs. The first profile is a profile that will slew the satellite in an optimal maneuver time duration, and the second profile is a profile that will maneuver the satellite with efficient fuel consumption. An input shaper to generate the command for rest-to-rest slew maneuvers can be written in the following form:

$$\begin{Bmatrix} A_i \\ t_i \end{Bmatrix} = \begin{Bmatrix} A_1 & A_2 & \dots & A_n \\ t_1 & t_2 & \dots & t_n \end{Bmatrix}, \tag{16}$$

where $i = 1, \dots, n$, A_i is the amplitude of the ith impulse, t_i is the time location of the ith impulse, and n is an integer. Usually, t_1 is selected to be zero.

For the time-optimal command, the value of n in the input shaper can be an even or odd integer. The values of A_i for this shaper, that produce the positive or negative constant-amplitude of the command, can be expressed as

$$\begin{cases} A_1 = 1 \\ A_i = 2(-1)^{i-1} \quad (i = 2, 3, \dots, n-1). \\ A_n = 1(-1)^{n-1} \end{cases} \tag{17}$$

For the fuel-efficient command, n in equation (16) must be an even integer, and the values of A_i can be written as follows [14]:

$$\begin{cases} A_i = 1 & \left(i = 1, 3, \ldots, \frac{n}{2} - 1, \frac{n}{2} + 2, \frac{n}{2} + 4, \ldots, n\right) \\ A_i = -1 & \left(i = 2, 4, \ldots, \frac{n}{2}, \frac{n}{2} + 1, \frac{n}{2} + 3, \ldots, n - 1\right) \end{cases}. \tag{18}$$

Equations (17) and (18) lead to the command constraint equations for time-optimal shapers and fuel-efficient shapers, respectively. An example of equation (18) is demonstrated by Figure 5, where a step convolved with this type of input shaper results in a series of alternating sign, variable-width pulses.

The other constraint equations are the motion constraints of the satellite as an undeformed body. The satellite must maneuver to the desired attitude angle with zero final velocity. These values governed by equations (14) and (13) of the previous section set the attitude maneuvers of rigid body motion. Since the main purpose of input shaping is to limit the amount of residual vibration that occurs when the system reaches its desired setting point, the constraint equation limiting

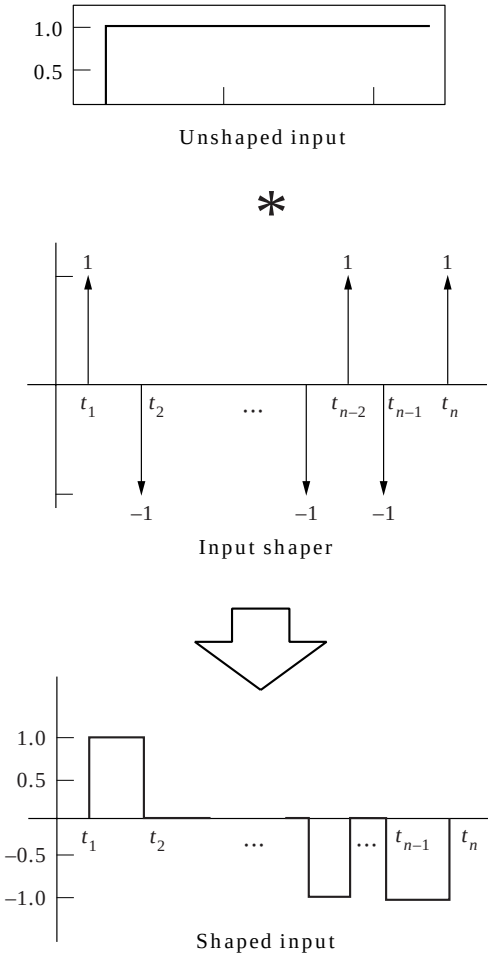

Figure 5. An example of input shaping to generate a series of alternating-sign pulses.

vibration amplitude must be defined. The constraint can be formulated as a ratio of residual vibration amplitude under a shaped input divided by residual vibration under an unshaped input. By expressing the constraint equation as a ratio, the value of residual vibration can be specified as a percentage of the vibration under unshaped command. A bang-bang command can be selected as the baseline unshaped command for rest-to-rest attitude maneuvers of the system with on–off actuators. As a note, the vibration under the bang-bang command will be zero when the width of the pulses is equal to a period of system vibration. If such a case occurs, the ratio can be formed relative to a step input.

A bang-bang command can be observed as a step input convolved with a shaper of the form

$$\begin{bmatrix} A_k \\ t_k \end{bmatrix} = \begin{bmatrix} 1 & -2 & 1 \\ 0 & t_2 & t_3 \end{bmatrix}, \tag{19}$$

where, in this expression, t_2 the switching time and t_3 is the length of the bang-bang. The bang-bang command is a time-optimal input for rest-to-rest maneuvers with three impulses.

When an undamped second-order system is subjected to a sequence of impulses, the amplitude of residual vibration can be formulated as a summation of the responses to individual impulses that is given in the reference [15]. The residual vibration amplitudes of the multimode flexible system such as the satellite studied here can be written in the following form:

$$R(\omega_m) = \sqrt{\left[\sum_{i=1}^{n} A_i \sin(\omega_m t_i)\right]^2 + \left[\sum_{i=1}^{n} A_i \cos(\omega_m t_i)\right]^2}, \quad m = 1, 2, \ldots, \tag{20}$$

where ω_m is an undamped natural frequency. The ratio of shaped to unshaped vibration can be defined by dividing equation (20) for the shaped command by its equivalent equation for the unshaped command. The percentage vibration relative to a bang-bang is

$$V(\omega_m) = \sqrt{\frac{\left[\sum_{i=1}^{n} A_i \sin(\omega_m t_i)\right]^2 + \left[\sum_{i=1}^{n} A_i \cos(\omega_m t_i)\right]^2}{\left[\sum_{k=1}^{3} A_k \sin(\omega_m t_k)\right]^2 + \left[\sum_{k=1}^{3} A_k \cos(\omega_m t_k)\right]^2}}, \tag{21}$$

where A_k and t_k describe the input shaper expressing the bang-bang command given by equation (19).

Then, equation (21) is used as the constraint equation to limit the residual vibration to an expected level of V at the system's frequency ω_m. The determination of V depends on the vibration amplitude as a result of the bang-bang and the expected residual vibration amplitude under the shaped command. If the vibration of the bang-bang is too large, while the expected vibration level is small enough, then V must be set to a very small value. The known zero

vibration (ZV) and zero vibration and derivative (ZVD) shapers use the criteria of $V = 0$.

5. REST-TO-REST ATTITUDE MANEUVER UNDER TIME-OPTIMAL/ FUEL-EFFICIENT SHAPED INPUTS

Singhose *et al*. [14] demonstrated that, for a simple system model consisting of two masses (m_1 and m_2), and a spring (k) with parameter values $m_1 = m_2 = k = 1$, fuel-efficient shaped command profiles spend smaller amounts of fuel compared with time-optimal profiles, while time lengths needed for maneuvers are relatively the same. Hence, is very useful to use the fuel-efficient shaped commands to control such a model, where the number of flexible modes is low and there is no limitation in the flexible mode deflection. However, for the complex system such as the satellite studied in this paper, the result has not been known yet. On the one hand, the satellite has a lot of flexible modes, while it must have high accuracies in pointing after the attitude maneuvers. On the other hand, since it is known that large structural deflections induce large internal loads, the deflections of flexible modes of the satellite must be kept small. In the system having a lot of flexible modes such as the finite element model of the satellite studied here, when the vibration at a natural frequency with the largest residual vibration is suppressed, for example to zero, other frequencies can amplify the resulting residual vibration. Thus, the final vibration that occurs is still relatively large and may still surpass the expected level of vibration in relation to its mission. In such a case, the vibration at several natural frequencies needs to be reduced until the resulting vibration remains below the acceptable level. In this section, the attitude maneuvers of the satellite under time-optimal and fuel-efficient shaped torque inputs will be simulated numerically.

The desired maneuver of the satellite observed in this study is 5° roll angle displacement, and the residual oscillations are determined to be not greater than 0·07° in roll and pitch angles, and not greater than 0·2° in yaw angle. These values of residual angle oscillations are the same as the permissible maximum antenna beam pointing errors of the satellite required by the KOREASAT [8]. When bang-bang torque inputs are used for the maneuver, as described in section 3, the very strong residual roll and yaw oscillations happen at $\omega = 0{\cdot}3593$ rad/s (see Figure 3), and these residual oscillations are caused by the roll input. The short time yaw bang-bang input use has small enough contribution to the residual attitude oscillation (see Figure 4). In view of the above, in order to satisfy the satellite mission, an input shaper is applied to the roll torque only, while the bang-bang yaw input is still applied. The inputs are applied to the satellite separately. The shaped roll input is applied first, and after that, the bang-bang yaw input is given. Remembering that the permissible maximum amplitude of roll oscillation is 0·07°, while the oscillation caused by the application of the bang-bang yaw input is about 0·04°, the resulting residual oscillation by the shaped roll input must be smaller than 0·03° (or 0·4% of the result of bang-bang roll input). In order to achieve this value, the input shaper with the same constant-amplitude roll torque input of 20 N-m is developed in

this study by setting V, equation (21), to zero at $\omega = 0{\cdot}3593$ rad/s. Besides this natural frequency, V at one of the other higher frequencies of the satellite (i.e., 0·9563 or 1·1166 rad/s) will be set to a small value. In this study, the number of impulses of input shapers is selected to be 8, so that the optimal-time input shaper is in the following configuration:

$$\begin{bmatrix} A_i \\ t_i \end{bmatrix} = \begin{bmatrix} 1 & -2 & 2 & -2 & 2 & -2 & 2 & -1 \\ 0 & t_2 & t_3 & t_4 & t_5 & t_6 & t_7 & t_8 \end{bmatrix}, \tag{22}$$

while the fuel-efficient input shaper is in the following form:

$$\begin{bmatrix} A_i \\ t_i \end{bmatrix} = \begin{bmatrix} 1 & -1 & 1 & -1 & -1 & 1 & -1 & 1 \\ 0 & t_2 & t_3 & t_4 & t_5 & t_6 & t_7 & t_8 \end{bmatrix}. \tag{23}$$

The value of t_1 has been selected to be zero in equations (22) and (23). The time-optimal inputs always consume the fuel during the maneuver duration, while in the fuel-efficient inputs there are periods where the fuel is not needed. In the fuel-efficient commands generated by equation (23), the fuelling periods happen at t_1–t_2, t_3–t_4, t_5–t_6, and t_7–t_8; and the non-fuelling period at t_2–t_3, t_4–t_5, and t_6–t_7. When a time duration of command is determined to be shorter than 30 s, four configurations of shaped inputs can be chosen, as listed in Table 3. In this table, the last two columns express percentages of vibration at two higher natural frequencies of the system, 0·9563 and 1·1166 rad/s. Besides constraints of the satellite rigid body motion, $t_8 < 30$, and $V(0{\cdot}3593) = 0$, shaped commands listed in Table 3 were obtained by using the following addition constraints: (i) $V(0{\cdot}9563) < 0{\cdot}2$, $1 < V(1{\cdot}1166) < 1{\cdot}5$, minimize $V(0{\cdot}9563)$, and minimize t_8; or (ii) $V(1{\cdot}1166) < 0{\cdot}2$, $1 < V(0{\cdot}9563) < 1{\cdot}5$, minimize $V(1{\cdot}1166)$, and minimize t_8. These selections are directed to locate at which natural frequencies besides 0·3593 rad/s will the vibration amplitude of the satellite be large. The first case of time-optimal command and the second case of fuel-efficient command have $V(1{\cdot}1166) < 0{\cdot}2$; while the second case of time-optimal command and the first case of fuel-efficient command have $V(0{\cdot}9563) < 0{\cdot}2$.

TABLE 3

Time location of impulses for shaping the roll torque inputs

Case number	t_1 (s)	t_2 (s)	t_3 (s)	t_4 (s)	t_5 (s)	t_6 (s)	t_7 (s)	t_8 (s)	$V(0{\cdot}9563)$ (%)	$V(1{\cdot}1166)$ (%)
Time-optimal 1	0	5·94	9·63	13·89	19·63	20·99	23·32	23·52	144	10·4
Time-optimal 2	0	4·89	8·01	12·93	18·56	20·98	24·58	24·70	18·5	148
Fuel-efficient 1	0	2·49	9·83	12·70	15·07	18·10	25·31	27·64	16·9	117·5
Fuel-efficient 2	0	2·18	8·43	10·63	17·47	19·65	25·90	28·10	128·0	12·8

5.1. RESIDUAL ROLL OSCILLATION

The roll angle motions of the main rigid body of the satellite for all cases are plotted in Figure 6. We can see in Figure 6(a) that the rest of the roll angle has been changed successfully to the desired new value of 5° after attitude maneuvers. The residual roll angle oscillation after maneuver resulting from the first case of time-optimal, where $V(0{\cdot}9563) = 144\%$ and $V(1{\cdot}1166) = 10{\cdot}4\%$, has a total amplitude of about 0·061°, or about 0·9% of the result of bang-bang input. This value satisfies the precision requirement of the satellite pointing. The second case of time-optimal with $V(0{\cdot}9563) = 18.5\%$ and $V(1{\cdot}1166) = 148\%$ gives the resultant amplitude of residual roll angle oscillation of about 0·57°, or 8·5% of the result of bang-bang input. This value is greater than the permissible maximum roll error of the satellite pointing. For the first case of fuel-efficient, where $V(0{\cdot}9563) = 16.9\%$ and $V(1{\cdot}1166) = 117{\cdot}5\%$, the resulting residual roll oscillation is large enough. Its resultant amplitude is about 0.45°, and the oscillation occurs largely at the period of 5·63 s (or $\omega = 1{\cdot}1166$ rad/s). This means that the input reduces the residual roll angle oscillation at about 6·7% compared with the result of the bang-bang input, but it is still greater, about 6·4 times, than its permissible maximum error. The second case of fuel-efficient with $V(0{\cdot}9563) = 128\%$ and $V(1{\cdot}1166) = {\cdot}12.8\%$ gives favorable residual roll angle

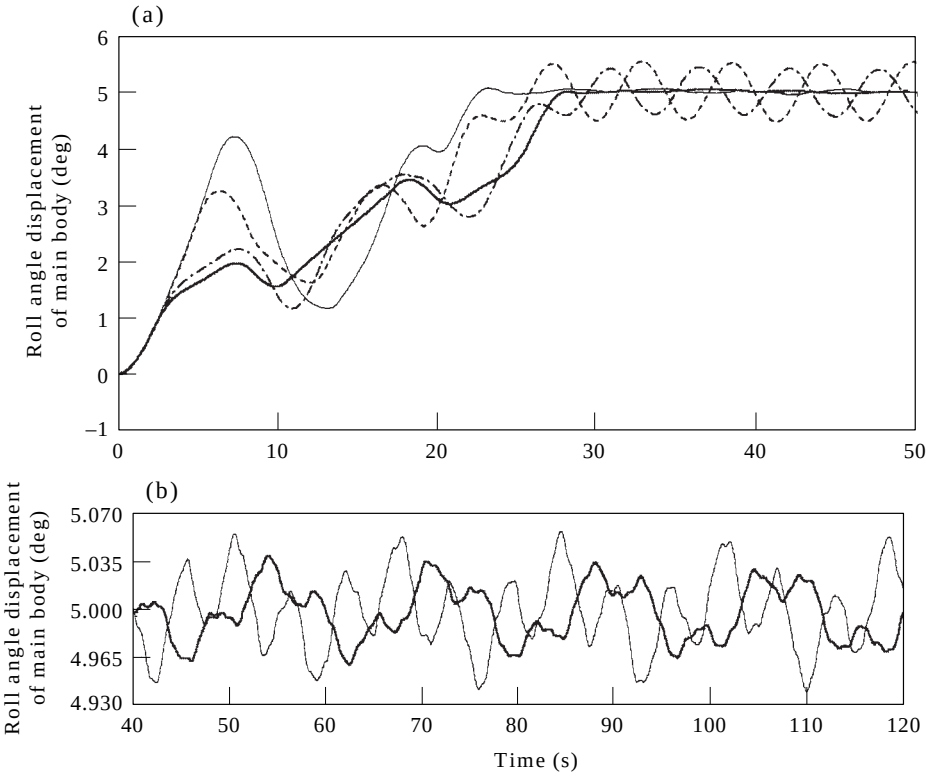

Figure 6. Time responses of roll angle displacement of the main body: (a) during maneuver; (b) residual oscillation. —, Time-optimal 1; - - -, time-optimal 2; - · - ·, fuel efficient 1; —, fuel-efficient 2.

oscillation. The resultant amplitude is about 0·041° (i.e., about 0·6% of the result of bang-bang input), which is smaller than the permissible maximum pointing error in roll.

Taking into account the percentages of vibration at $\omega = 0{\cdot}9563$ and 1·1166 rad/s calculated in each case in connection with their resultant residual roll oscillations, the model of the satellite observed in this study has a tendency to give a larger response amplitude at 1·1166 rad/s compared with the 0·9563 rad/s one. Besides its 0·3593 rad/s natural frequency, one must set the percentage vibration at 1·1166 rad/s to a small value in selecting shaped inputs in order to achieve residual roll oscillation in the expected level.

5.2. RESIDUAL PITCH AND YAW OSCILLATIONS

For all cases of switching time listed in Table 3, the pitch angles are undisturbed during and after the maneuvers, as shown in Figure 7. The rests of yaw angles after the maneuvers are still zero. The first case of time-optimal gives the largest maximum yaw angle displacement during the attitude maneuver, at about 1·75°. The large residual yaw oscillations occur in the second case of time-optimal and the first case of fuel-efficient, as seen in Figure 7(a). Their total amplitudes of residual yaw oscillations are about 0·35° and 0·28°, which are

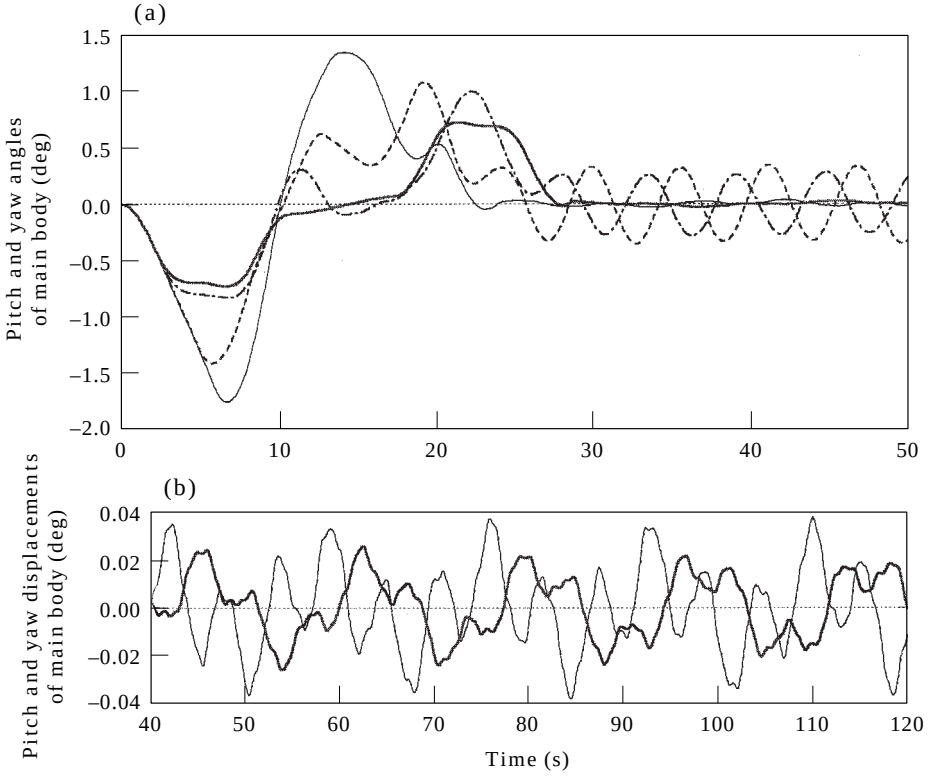

Figure 7. Time responses of pitch and yaw angle displacements of the main body: (a) during maneuver; (b) residual oscillation. —, Yaw, time-optimal 1; - - -, yaw, time-optimal 2; - · -, yaw, fuel-efficient 1; —, yaw, fuel efficient 2; · · · · ·, pitch.

greater than the permissible maximum pointing error in yaw. The total amplitudes of the first case of time-optimal and second case of fuel-efficient are smaller than 0·04°, as seen in Figure 7(b), and these values are smaller than the permissible maximum pointing error in yaw described previously. The total amplitude of residual yaw oscillation in the second case of fuel-efficient is the smallest one. The yaw motions are the coupling motions of their roll ones. These phenomena can be seen in the responses of all cases, comparing Figures 6(b) and 7(b), in which both the response shapes and same periods of oscillation appear sharply.

5.3. MAXIMUM DEFLECTIONS OF SOLAR PANELS

Since the solar panels of the satellite are supposed to have only out-of-plane elastic deformations, the deflections of their nodes are symmetric with respect to Y_b and antisymmetric with respect to X_b. This means that the deflection of node 25 at each observation is the same as node 27, and the deflections of nodes 52 and 54 have the same magnitude but in the opposite direction. The maximum deflections of solar panels happen at their tips, i.e., nodes 25, 27, 52, and 54, and as a representation, in this paper, time responses of node 25 are given in Figure 8. The first case of time-optimal input where the sequence impulsing time intervals of the input shaper in the range of 0·20 to 5·94 s gives the largest

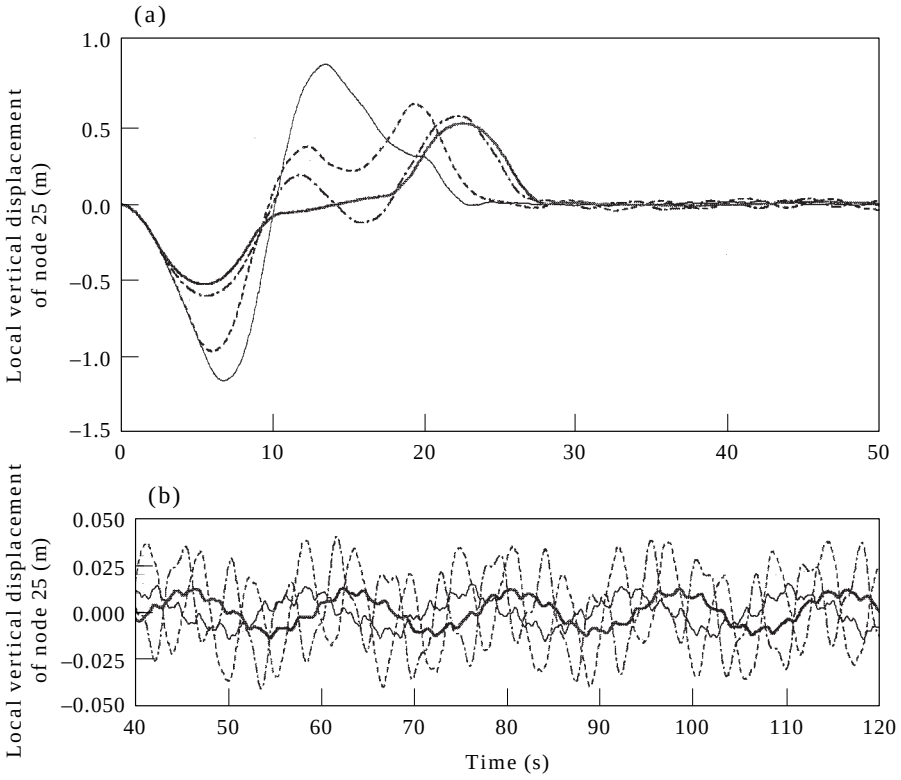

Figure 8. Time responses of local vertical displacement of node 25 of the solar panel. (a) during maneuver; (b) residual vibration. Key as for Figure 6.

maximum deflection of node 25, as seen in Figure 8(a), about 115·7 cm downward at $t = 6.75$ s. Compared with the length of the solar panel, this deflection is large enough, at about 9·64%. The second case of time-optimal input with the sequence impulsing time intervals from 0·12 to 5·63 s gives the maximum deflection of this node at about 95·9 cm downward at $t = 5{\cdot}98$ s. The first case of fuel-efficient input, where the fuelling time segment lengths of the input shaper are in the range of 2·33 to 3·03 s, gives the largest maximum deflection of node 25 as seen in Figure 8(a), about 59·5 cm downward at $t = 5{\cdot}56$ s. Compared with the length of the solar panel, this deflection is only about 4·96%. The second case of fuel efficient input with the fuelling segment lengths from 2·18 to 2·20 s gives the 52·8 cm maximum deflection upward of this node at $t = 22{\cdot}61$ s. Since it is known that the time-optimal inputs always use the fuel, it can be seen that in both kinds of shaped inputs being applied the larger the value of the longest fuelling time segment length, the larger the maximum deflection on the solar panel will be. The total amplitudes of residual vibration of node 25 for all cases are smaller than 4·2 cm, as shown in Figure 8(b).

5.4. MAXIMUM RESIDUAL VIBRATION OF SOLAR PANELS

The use of shaped inputs has reduced successfully the residual vibrations of flexible modes. The maximum residual vibrations of solar panels for the first case of time-optimal happen at nodes 19, 21, 46, and 49; the second case of time-optimal and first case of fuel-efficient happen at nodes 16, 18, 43, and 45; while for the second case of fuel-efficient, they happen at their tips, i.e., nodes 25, 27, 52, and 54. In the time-optimal maneuvers, the total amplitude of the largest residual vibration of panels of the first case is 1·6 cm (about 0·14% of the solar panel's length), and the second one is 17·6 cm (1·47% of the solar panel's length), as shown in Figure 9. In the fuel-efficient maneuvers, the amplitude of the first case is 14·3 cm (or 1·19% of the solar panel's length), and the second one is 1·4 cm (0·12% of the solar panel's length). As in the resulting residual roll and yaw oscillations, the second case of fuel-efficient also gives the smallest value in the resulting maximum residual vibration of solar panels.

5.5. AMOUNT OF FUEL BEING CONSUMED

The maneuvers under the time-optimal inputs always consume the fuel during the applications of inputs. If the fuel needed in the fuelling period is 1 unit of mass per second, the first case where its maneuver satisfies the requirement of the satellite in pointing accuracies consumes 23·52 mass units of fuel, while the second case consumes 24·70 mass units. In the fuel efficient maneuvers, the fuel is only consumed in the fuelling periods. The first case of this maneuver consumes 10·72 mass units, while the second case which satisfies the requirement of pointing accuracies after maneuver needs 8·72 mass units of fuel. This means that the second case of fuel-efficient inputs consumes only 37·1% of fuel needed in the first case of time-optimal inputs, while the maneuver duration is 19·5% longer.

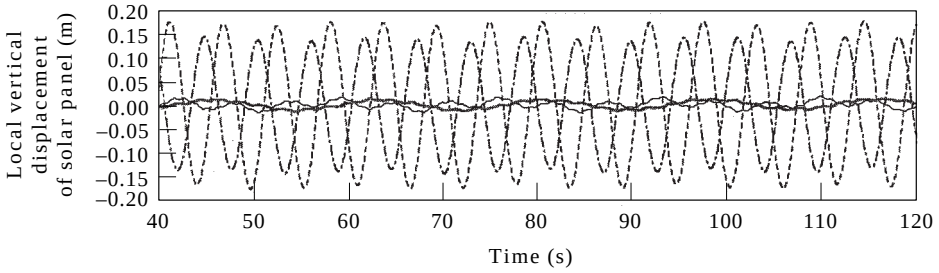

Figure 9. Time responses of the largest residual vibration of the solar panel for all cases. —, Node 19, time-optimal 1; - - -, node 16, time-optimal 2; - · -, node 16, fuel-efficient 1; ▬, node 25, fuel efficient 2.

6. CONCLUDING REMARKS

Attitude maneuvers of the flexible satellite induce the vibration of flexible members as well as satellite libration motion. However, for the satellite in symmetrical conditions with respect to the Y_b-axis of the rigid main body fixed frame—i.e., I_{xy} and I_{yz} equal to zero—under the roll and yaw torque inputs, pitch motions are not induced. Without shaping the input, the flexible satellite has poor attitude accuracy after slew maneuver. Under the combination of bang-bang roll and yaw torque input, for 5° desired roll angle displacement only, the satellite studied in this paper has residual roll angle oscillation with amplitudes greater than the changing of the desired new rest angle. Shaped inputs show their capability to reduce residual oscillation and vibration. For the shaped inputs with eight impulses compared here, the maximum total amplitudes of residual roll oscillation become smaller than 0·57°, the largest total amplitudes of residual vibration of 12 m of solar panel are not greater than 17·6 cm, and the total amplitudes of tip solar panel's residual vibration are not greater than 4·2 cm.

The selection of shaped input with $V = 0$ at ω of the strongest residual vibration and relatively small V at other strong ones can give the attitude maneuver with residual oscillations of attitude angles at the expected levels.

The maximum deflections of flexible members during maneuvers depend on the length of time segment of fuelling. If this segment is long, the maximum deflection will be long too. To maneuver flexible spacecraft in small maximum deflection, the input shaper consisting of short time segments of fuelling is needed.

For the same number of impulsing times in a limited maneuver time duration, the use of fuel-efficient commands will give smaller maximum deflections of flexible members and consumes a smaller amount of fuel compared with the time-optimal commands. Thus, the use of fuel-efficient commands is recommended for maneuvers under constant-amplitude shaped inputs.

REFERENCES

1. N. C. Singer and W. P. Seering 1990 *Journal of Dynamic Systems, Measurement and Control* **112**, 76–82. Preshaping command inputs to reduce system vibration.

2. K. ROGERS and W. P. SEERING 1996 *AIAA Guidance, Navigation, and Control Conference, San Diego, CA*. Input shaping for limiting loads and vibration in systems with on–off actuators.
3. Q. LIU and B. WIE 1992 *Journal of Guidance, Control, and Dynamics* **15,** 597–604. Robust time-optimal control of uncertain flexible spacecraft.
4. T. SINGH and S. R. VADALI 1994 *Journal of Guidance, Control, and Dynamics* **17**, 346–353. Robust time-optimal control: a frequency domain approach.
5. B. WIE, R. SINHA, and Q. LIU 1993 *Journal of Guidance, Control, and Dynamics* **15**, 980–983. Robust time-optimal control of uncertain structural dynamic systems.
6. L. Y. PAO and W. E. SINGHOSE 1995 *IEEE Conference on Control Applications, Albany, NY*, 875–881 *New York: Institute of Electrical and Electronics Engineers*. A comparison of constant and variable amplitude command shaping techniques for vibration redution.
7. W. E. SINGHOSE, A. K. BANERJEE and W. P. SEERING 1997 *Journal of Guidance, Control, and Dynamics* **20**, 291–298. Slewing flexible spacecraft with deflection-limiting input shaping.
8. H. HWANGBO 1992 *AIAA, A Collection of Technical Papers of the* 14*th International Communication Satellite Systems, Washington, DC* **1**, 550–555. The Korea domestic communications and broadcasting satellite system.
9. H. KOGUCHI and S. PARMAN 1995 *Proceedings of International Session—the* 72*nd JSME Spring Annual Meeting*, 70–73. The dynamics of a satellite with flexible solar panels: the vibration of solar panels approached to behave as structures with proportional damping.
10. H. KOGUCHI and S. PARMAN 1996 *Proceedings of International Session—the* 73*rd JSME Spring Annual Meeting* 75–78. Attitude dynamics of a satellite with flexible solar panels based on its nonlinear equations of motion.
11. H. KOGUCHI and S. PARMAN 1996 *Proceedings of the Third International Conference on Motion and Vibration Control, Tokyo, Japan* **3**, 382–387. Attitude dynamics of a satellite with flexible solar panels: comparison between the nonlinear equations and linearized equations of motion.
12. O. C. ZIENKIEWIEZ 1977 *The Finite Element Method*. New York: McGraw-Hill; third edition.
13. F. K. BOGNER, R. H. MALLET, M. D. MINICK and L. A. SCHMIDT 1965 *Development and Evaluation of Energy Search Methods of Nonlinear Structural Analysis*. Flight Dynamics Laboratory Report, AFFDL TR 65–113.
14. W. SINGHOSE, K. BOHLKE and W. SEERING 1995 *Proceedings of the* 1995 *AIAA Guidance, Navigator, and Control Conference*. Fuel-efficient shaped command profiles for flexible spacecraft.
15. R. E. BOLZ and G. L. TUVE 1973 *CRC Handbook of Tables for Applied Engineering Science*, 1071. Boca Raton, FL: CRC Press.